Article

Geochemical Characterization of Zircon in Fyfe Hills of the Napier Complex, East Antarctica

Mami Takehara [1],*, **Kenji Horie** [1,2] **and Tomokazu Hokada** [1,2]

1   National Institute of Polar Research, 10-3, Midori-cho, Tachikawa-shi, Tokyo 190-8518, Japan;
    horie.kenji@nipr.ac.jp (K.H.); hokada@nipr.ac.jp (T.H.)
2   Department of Polar Sciences, The Graduate University for Advanced Studies, SOKENDAI, 10-3,
    Midori-cho, Tachikawa-shi, Tokyo 190-8518, Japan
*   Correspondence: takehara.mami@nipr.ac.jp

Abstract: Ultra-high temperature (UHT) metamorphism plays an essential role in the development and stabilization of continents through accretionary and collisional orogenesis. The Napier Complex, East Antarctica, preserves UHT metamorphism, and the timing is still debated. U–Pb zircon geochronology integrated with rare earth element (REE) and oxygen isotope was applied to a garnet-bearing quartzo-feldspathic gneiss to confirm the timing of UHT metamorphism in Fyfe Hills in the western part of the Napier Complex. The zircons are analyzed using a sensitive high-resolution ion microprobe (SHRIMP). The cathodoluminescence observation and U–Pb ages allowed us to classify the analytical domains into three types: inherited domains (Group I), metamorphic domains (Group II), and U–Pb system disturbed domains (Group III). The REE patterns of Group II are characterized by a weak fractionation between the middle REE and heavy REE, which reinforces the above classification. The $^{207}Pb^*/^{206}Pb^*$ ages of Group II have an age peak at 2501 Ma, therefore, the gneiss experienced high temperature metamorphism at 2501 Ma. $\delta^{18}O$ of zircons are homogeneous among the three groups (5.53 ± 0.11‰, 5.51 ± 0.14‰, and 5.53 ± 0.23‰), which suggests re-equilibration of oxygen isotopes after metamorphism at ca. 2501Ma under dry UHT conditions.

Keywords: U–Pb geochronology; zircon; REE pattern; $\delta^{18}O$; Napier Complex

1. Introduction

Ultra-high temperature (UHT) metamorphism is critical to understanding the large-scale tectonic processes affecting the deep crust and lithosphere throughout Earth history. The UHT metamorphism is recognized at over 60 areas or localities [1]. The Napier Complex in East Antarctica is the location where the regional UHT metamorphism was first recognized [2] and experienced extremely high temperatures (>1100 °C) based on the mineral assemblage of sapphirine + quartz ([3] and reference therein). The thermal history of the Napier Complex is important for unraveling the Earth's crustal evolution, including deep crust; however, geochronological constraints, such as the timing and duration of the metamorphic events, are still debated. Two hypotheses for the timing are proposed in previous studies: (i) the UHT metamorphism occurred no earlier than 2840 Ma and possibly from 2590 to 2550 Ma [4–8], (ii) it occurred from around 2500 to 2450 Ma [9–14].

Geochronological studies of the Napier Complex have been performed mainly via the U–Pb zircon method [4–14]. Zircon, which is one of the most common minerals used for U–Th–Pb isotope dating, also provides an opportunity for integration between age and geological processes. The partitioning of heavy rare earth elements (HREE) between zircon and garnet has been considered as the most robust method for evaluating the relationship between zircon and garnet during metamorphic events [15–17]. Oxygen isotopes in zircon also provide useful information about magmatic evolution,

genesis of magmas, isotope exchange between zircon and surrounding minerals during metamorphism, hydrothermal alteration, etc. [18]. Recent studies also reported the data of variable trace elements in zircon for assessing ancient lithosphere, hydrosphere, and atmosphere interactions [19–21].

In this study, we focus on the garnet-bearing quartzo-feldspathic gneiss, collected from Fyfe Hills in the Napier Complex, to verify and obtain new insights about the timing of the UHT metamorphism. Multiple U–Pb ages in the sample have already been reported by [9]. Zircon grains were selected from the sample and analyzed using a sensitive high-resolution ion microprobe (SHRIMP-IIe). We suggest a new interpretation of the multiple U–Pb ages in the Fyfe Hills sample by combining the U–Pb age, cathodoluminescence images, rare earth elements (REE) compositions, and oxygen isotope ratio.

2. Materials and Methods

2.1. Geological Background

The Napier Complex consists of coastal outcrops, islands, and inland mountain ranges in Enderby Land, East Antarctica (Figure 1). Archean crustal records have been collected at several localities of the Napier Complex ([8] and references therein). The Napier Complex is composed of various granulite-facies metamorphic rocks, such as tonalitic–trondhjemitic–granodioritic (TTG) orthogneisses, granitic gneisses, mafic granulites, and paragneisses. These granulite-facies metamorphic rocks have been affected by multiple thermal events, including UHT metamorphism in the latest Archean Era. The peak temperature of the UHT metamorphism is estimated to be above 1100 °C [22–24]. SHRIMP U–Pb zircon analysis has revealed the Eoarchean protolith ages (>3.7 Ga) from Mt. Sones [25–27], Gage Ridge [6,27–29], Mt. Jewell, and Budd Peak [8]. Conversely, the ages of most of the rocks in the Napier Complex other than these Eoarchean outcrops were derived from magmatic precursors with mid- to late-Archean ages of ca. 3300–2600 Ma.
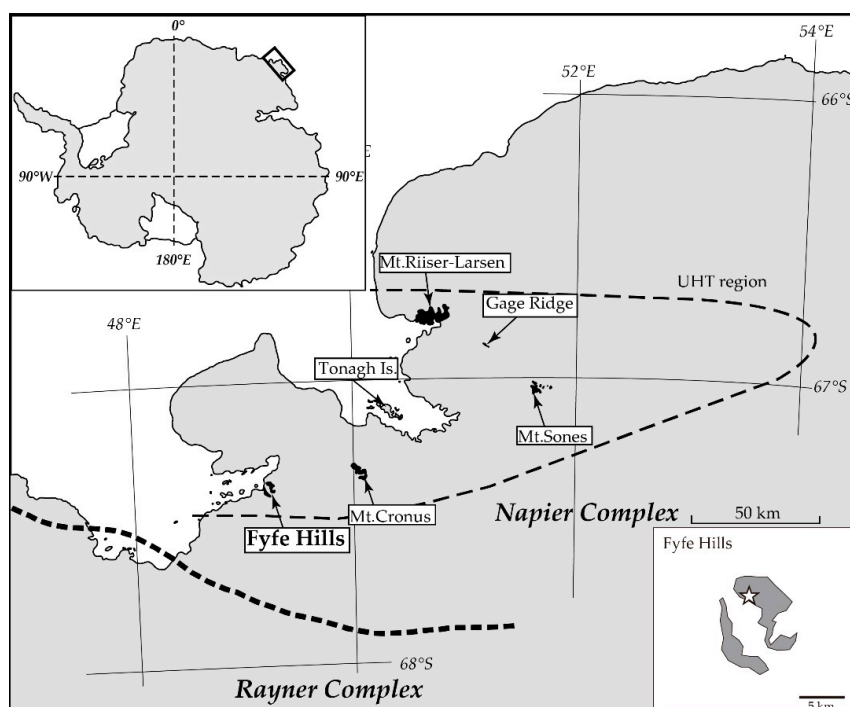

Figure 1. Geological outline of the Napier Complex, Enderby Land, East Antarctica, modified after [9]. The ultra-high temperature (UHT) region, indicated by a broken line, is composed of sapphirine + quartz in isograd. Bold broken line shows the position of the boundary between the Napier Complex and the Rayner Complex. Black dots indicate outcrops. In the bottom-right inset, the star indicates the approximate location of the YH05021606A sample.

Fyfe Hills, at which the sample was collected, is located 50–100 km west of Mt. Sones and Gage Ridge and situated within a UHT region defined by the occurrence of sapphirine + quartz paragenesis ([9] and references therein).

2.2. Sample

The garnet-bearing quartzo-feldspathic gneiss, YH05021606A, was collected from Fyfe Hills, and the sampling location was E 49°11.533′, S 67°20.875′. The felsic gneiss is mainly composed of garnet + mesoperthite (ternary feldspar) + quartz, with small amounts of zircon and opaque minerals [9]. The constituent minerals show a granoblastic texture. Garnet is porphyroblastic, and its grain size varies from <1 to 3 mm in diameter (Figure 2). Hydrous minerals are typically lacking in the rock, which is consistent with the >900 °C UHT metamorphic conditions. The sample was collected by Y.H. during fieldwork on the 2004–2005 Japanese Antarctic Research Expedition. Because the field survey in these areas was conducted in a short time, the field relationship of these samples is not clear [9]. The zircon U–Pb ages of the YH05021606A sample have already been reported in [9] and show multiple age peaks centered at ca. 3025, 2943, 2883, 2818, 2759, 2674, 2518, and 2437 Ma.
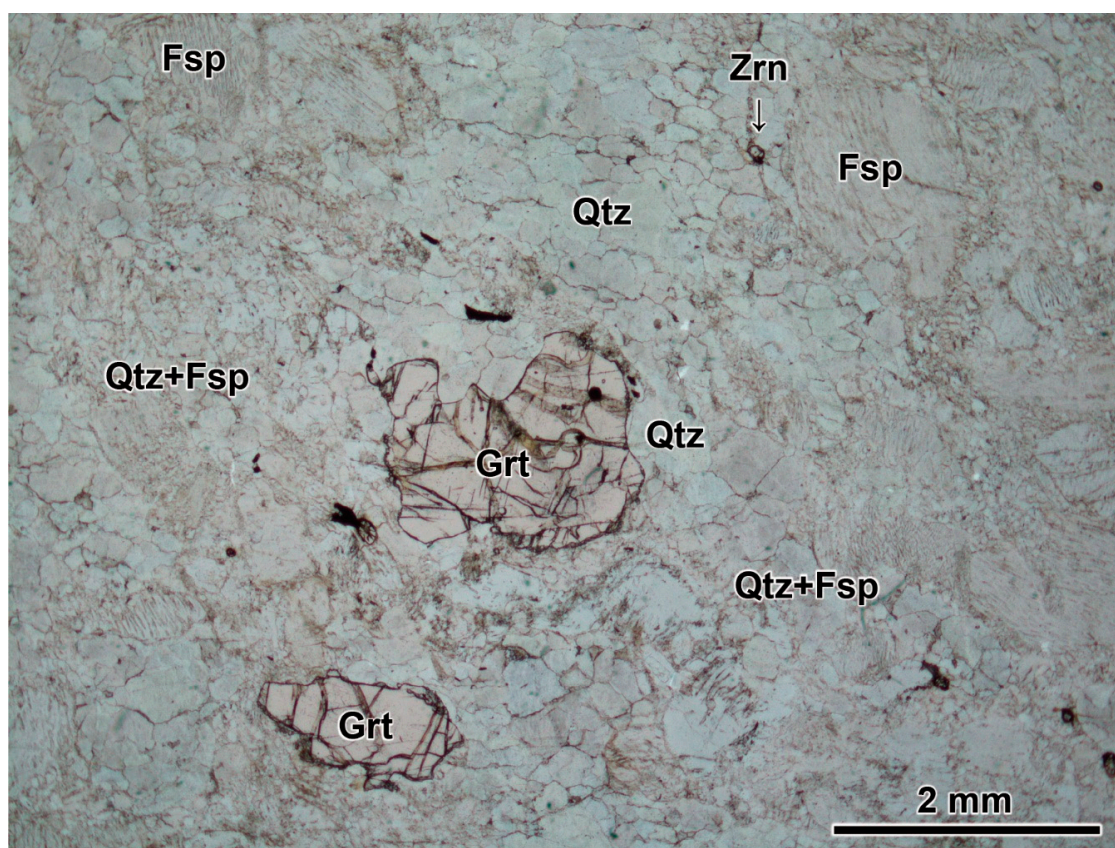
Figure 2. Plane-polarized light photomicrograph of YH05021606A. Mineral abbreviations are as follows. Qtz: quartz, Fsp: ternary feldspar (mesoperthite), Grt: garnet, Zrn: zircon.

2.3. Analytical Methods

A high-voltage pulse power fragmentation device (SELFRAG Lab.) at the National Institute of Polar Research, Tachikawa, Japan (NIPR), was used for the original rock fragmentation of YH05021606A to collect zircons without modifying their external morphologies and to avoid contamination during rock pulverization. Rocks of approximately 250 g were pulverized using a voltage of 120 kV and a disposable sieve with a 710 μm mesh. The detailed pulverization procedure can be found in [30]. After pulverizing the samples, zircon grains were separated using conventional mineral separation

techniques, including heavy liquid separation with methylene iodide and magnetic separation with a Nd-magnet. Approximately 500 zircon grains were handpicked from the sample. The external morphologies of the collected zircon grains were observed in the low vacuum mode of a scanning electron microscope (LV-SEM; JEOL JSM-5900LV) at the NIPR. To investigate the chemical properties of UHT zircon, the most transparent 67 zircon grains were mounted together with reference zircons in an epoxy resin disc. After curing, the grain mount was polished using 15 μm, 6 μm, 3 μm, and 1μm diamond pastes on a slow-speed rotating disk along a cross-section through the grains. Transmitted light images were obtained using an optical microscope. The backscattered electron (BSE) and cathodoluminescence (CL) images were obtained using the LV-SEM with a Gatan mini CL detector, used to observe the internal textures and mineral inclusions of the zircon grains and to select suitable analytical spots. The surfaces of the grain mounts were washed with diluted hydrochloric acid and ultrapure water to remove any lead contamination from the zircon surfaces. The grain mount was then coated with gold before U–Pb analyses that were done using a sensitive high-resolution ion microprobe (SHRIMP-IIe). After U–Pb and REE analyses, the grain mount was polished to remove the U–Pb analytical spots and coated with aluminum for oxygen isotope analysis using a 5-head multicollector-type ion probe (SHRIMP-IIe/AMC). After the oxygen isotope analysis, true color CL images of the grain mount were obtained using a Gatan ChromaCL2 system installed with a field emission SEM (FE-SEM; JEOL JSM-7100F) at the NIPR.

U–Pb isotopic dating of zircon was conducted using SHRIMP-IIe at the NIPR. An O_2^- primary ion beam of 0.9–1.3 nA was used to sputter an analytical spot approximately 10 μm in diameter. TEMORA2 zircon (^{206}Pb*/^{238}U age = 416.8 $\pm$ 1.3 Ma; [31]) and FC1 zircon (^{206}Pb*/^{238}U age = 1099.9 $\pm$ 1.1 Ma; [32]) were used as reference materials for calibration of the ^{206}Pb*/^{238}U ratio, and 91,500 zircon (U concentration 81.2 ppm; [33]) was used for the calculation of the U concentration. The U–Pb data were reduced according to the procedure described in [34], using the SQUID2 Excel macro of [35]. Common Pb was corrected based on the measured ^{204}Pb and Pb growth model [36] and calculated with the Isoplot/Ex software [37]. The U–Pb data for zircon grains with a high U content (greater than 2500 ppm) were corrected following the method described in [38,39].

The REE abundances in zircons were determined using SHRIMP-IIe, using the same spots as the U–Pb analyses. An O_2^- primary ion beam of 1.0–1.5 nA was used to sputter an analytical spot approximately 10 μm in diameter. Mass peaks from ^{89}Y$^+$ to ^{180}Hf$^+$ were scanned under a high-mass-resolution mode (M/ΔM: ~9000) to prevent isobaric interferences from light REE oxide species onto heavy REE mono-atomic species [40–42]. The counts for each element are referenced to ^{96}Zr$^+$ derived from the matrix component of zircon. To calculate the elemental abundances of REE, 91,500 zircon [43] was used as the reference material.

The oxygen isotope compositions of the zircon grains were determined using SHRIMP-IIe/AMC at the NIPR, using the same positions as the U–Pb and REE analyses. After removing the analytical spots, the mount was coated with aluminum. The analytical procedure and configuration of the SHRIMP-IIe/AMC were similar to those described in [20,44]. A Cs$^+$ primary ion beam was used to sputter an analytical spot approximately 25 μm in diameter. The beam intensity was ~3.5 nA. The secondary ions (^{16}O$^-$ and ^{18}O$^-$) were collected using Faraday cups with widths of 300 μm, for a counting time of 10 s. The electron-induced secondary ion emission (EISIE [44]) was monitored three times during each analysis. Helmholtz coils were utilized to cancel out the effects of the Earth's magnetic field. TEMORA2 zircons (δ^{18}O = 8.20‰; [31]) mounted with the YH05021606A zircons were used as reference material for calibrating the instrumental mass fractionation. FC1 zircons (δ^{18}O = 5.4‰; [44]) mounted with YH05021606A zircons were also used for comparison.

3. Results

3.1. Zircon Description

The zircon grains in the sample have rounded shapes and are typically 150 μm in size. The grains contain small mineral inclusions of quartz and feldspar. CL images of typical zircon grains are shown in Figure 3. Approximately half of the zircon grains in the sample show core-rim structures with bright CL response rims of variable widths (10–50 μm) (Figure 3a,b). The cores are characterized by broad zoning with a dark CL response (Figure 3b), oscillatory zoning, or sector zoning (Figure 3a). The oscillatory- or sector-zoned cores are truncated by the rims, which is interpreted to indicate that the protolith contained igneous detritus [45]. The rims with bright CL responses are characterized by broad zoning (Figure 3a) or nebulous to fir-tree structures (Figure 3b) that define irregular boundaries with the cores. The other half of the zircon grains with no apparent core-rim structure can be divided into broad zoning with a dark CL response (Figure 3c), oscillatory zoning (Figure 3e), sector zoning (Figure 3d), broad zoning with bright CL response (Figure 3f), and nebulous to fir-tree zoning (Figure 3g). SHRIMP analyses were conducted on each domain (Table S1).

3.2. U–Th–Pb Zircon Geochronology

In this study, only concordant data, defined as <10% discordance (discordance = {1 − (^{206}Pb*/^{238}U age)/(^{207}Pb*/^{206}Pb* age)} × 100; [46]), were considered for age evaluation. A total of 90 spots on 66 zircon grains in the quartzo-feldspathic gneiss (Sample No. YH05021606A) were analyzed, and results are shown in the Tera-Wasserburg concordia diagram (Figure 4; Table S1). It shows the age range of 1978 Ma–2809 Ma. The U and Th contents in the zircons ranged from 161 ppm to 4712 ppm and from 35 ppm to 703 ppm, respectively. The broad zoned cores with a dark CL response have higher U contents (365–4712 ppm). The Th/U ratios in the rim and core are from 0.12 to 1.64 and from 0.03 to 1.60, respectively. The Th/U ratios of the non-core-rim structured grains with nebulous to fir-tree zoned textures (e.g., Figure 3g) and those with oscillatory or sector zoning (e.g., Figure 3e) are from 0.07 to 1.65 and 0.10 to 1.85, respectively. In this sample, there is no systematic difference in the Th/U ratios between the core and rim and between the nebulous to fir-tree zoned grains and oscillatory- or sector-zoned grains.

The U–Pb data in the sample reveal a wide age distribution, ranging from 1978 Ma to 2809 Ma in ^{207}Pb*/^{206}Pb* age (Figure 4; Table S1), and a probability density diagram of ^{207}Pb*/^{206}Pb* ages shows multiple age peaks (Figure 4). The major age peaks are centered at ca. 2809 Ma, 2596 Ma, 2533 Ma, 2501 Ma, 2423 Ma, 2380 Ma, 2267 Ma, 2189 Ma, 2100 Ma, 2008 Ma, and 1978 Ma (Figure 4). The age data obtained in this study are consistent with those reported in [9]; however, age peaks centered at 3025 Ma, 2943 Ma, 2759 Ma, and 2674 Ma were absent in the present study. Moreover, the age peaks younger than ca. 2400 Ma (2380 Ma, 2267 Ma, 2189 Ma, 2100 Ma, 2008 Ma, and 1978 Ma) were not reported in [9].
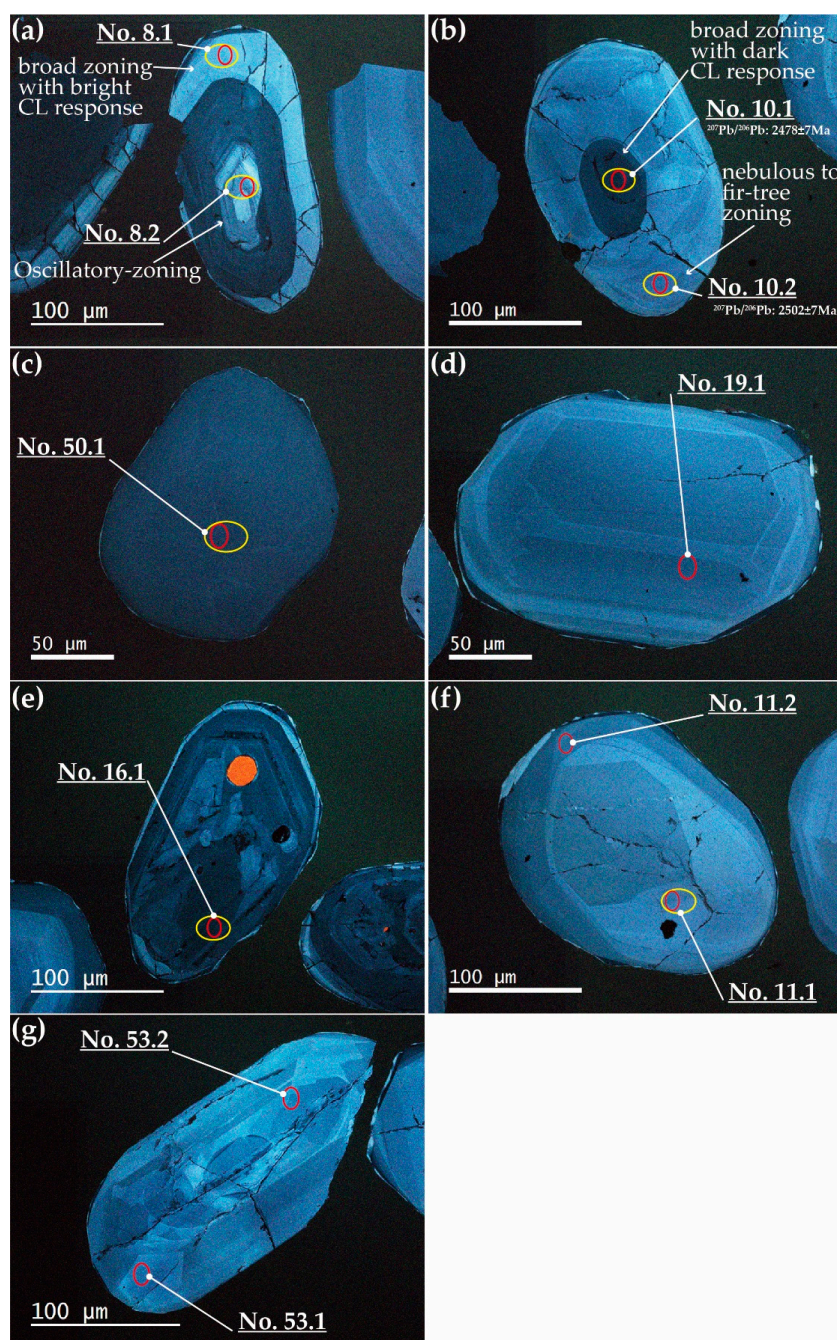
Figure 3. Cathodoluminescence (CL) images of YH05021606A zircons. The red-colored ellipses indicate the U–Pb and rare earth element (REE) analytical spots using a sensitive high-resolution ion microprobe (SHRIMP-IIe), and the yellow-colored ellipses indicate the oxygen isotope analytical spot using SHRIMP-IIe/AMC. (**a**) Grain no. YH1606A-8. Spot no. 8.1 is in a rim of broad zoning with a bright CL response. Spot no. 8.2 is in a core of oscillatory zoning; (**b**) grain no. YH1606A-10. Spot no. 10.1 is in a core of broad zoning with a dark CL response. Spot no.10.2 is in a rim of nebulous to fir-tree zoning; (**c**) grain no. YH1606A-50. Spot no. 50.1 is a grain of broad zoning with a dark CL response; (**d**) grain no. YH1606A-19. Spot no. 19.1 is a sector zoning grain; (**e**) grain no. YH1606A-16. Spot no. 16.1 is an oscillatory zoning grain; (**f**) grain no. YH1606A-11. Spot nos. 11.1 and 11.2 are a grain of broad zoning with a bright CL response; (**g**) grain no. YH1606A-53. Spot nos. 53.1 and 53.2 are a nebulous to fir-tree zoning grain.
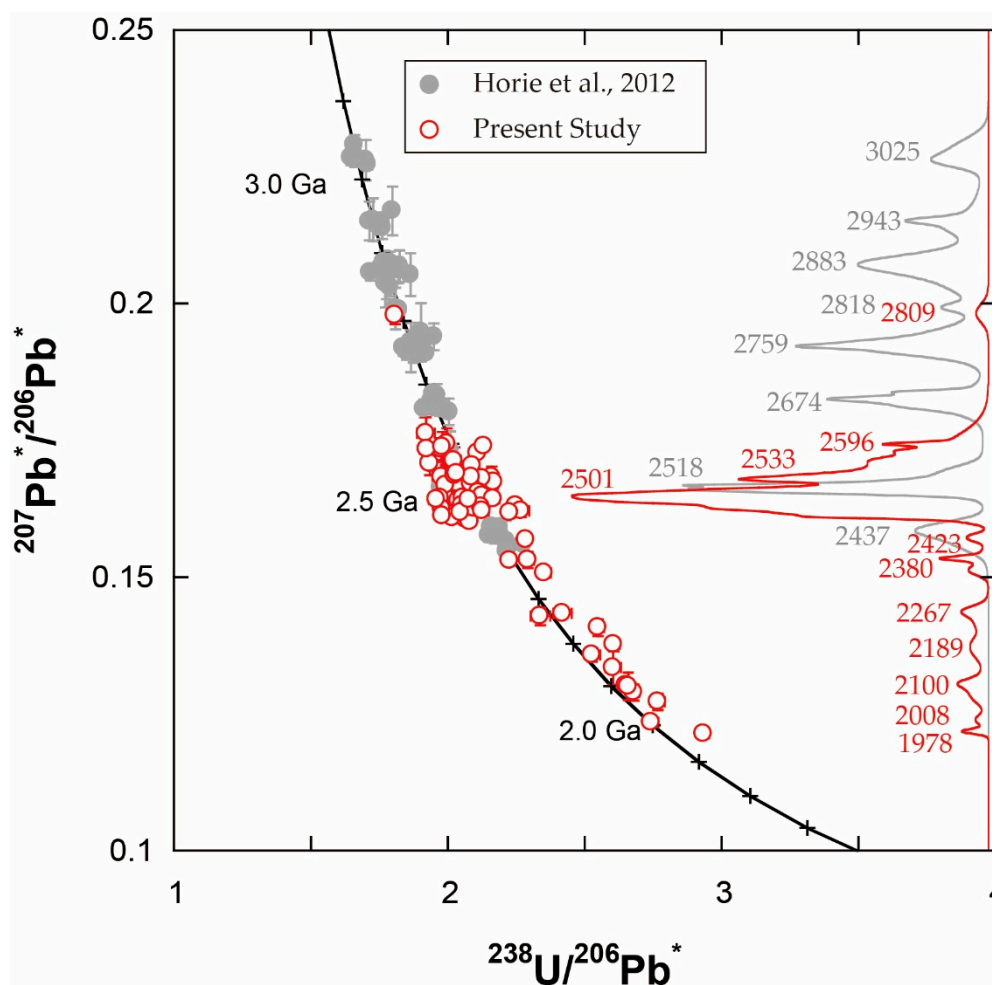
Figure 4. Tera-Wasserburg concordia diagram with a probability density diagram of ^{207}Pb*/^{206}Pb* age of the YH05021606A zircons. Error bars are 1σ. The gray-colored plots are derived from [9].

3.3. REE Content in Zircon

The results are listed in Table S2. Typical REE abundance patterns normalized by C1-chondrite values [47] of YH05021606A zircons are shown in Figure 5. The REE patterns of the zircons are characterized by a large fractionation between light REE (LREE: La, Pr, and Nd) and heavy REE (HREE: Tm, Yb, and Lu), positive Ce anomalies, and negative Eu anomalies. The REE patterns obtained from the rims are characterized by a weak fractionation between middle REE (MREE: Gd, Tb, and Dy) and HREE (HREE/MREE = 0.41–1.53) rather than those of the cores (HREE/MREE = 1.10–10.44) (Table S2). In the cores, the REE patterns show a wider variation in LREE to HREE (HREE/LREE = 32–1491), especially negative Eu anomalies (Eu/Eu* = 0.016–0.379; Eu* is defined as (Sm + Gd)/2 in the normalized REE patterns [41]) (Figure 5; Table S2). The REE patterns of the non-core-rim structured grains with oscillatory or sector zoning (HREE/MREE = 0.49–7.29, HREE/LREE = 34–1505, and Eu/Eu* = 0.014–0.617) are similar to those of cores (Figure 5; Table S2). Those of the non-core-rim structured grains with nebulous to fir-tree zoned textures (HREE/MREE = 0.23–1.98, HREE/LREE = 9–159, and Eu/Eu* = 0.014–0.078) are similar to those of rims (HREE/MREE = 0.41–1.53, HREE/LREE = 11–133, and Eu/Eu* = 0.014–0.234).
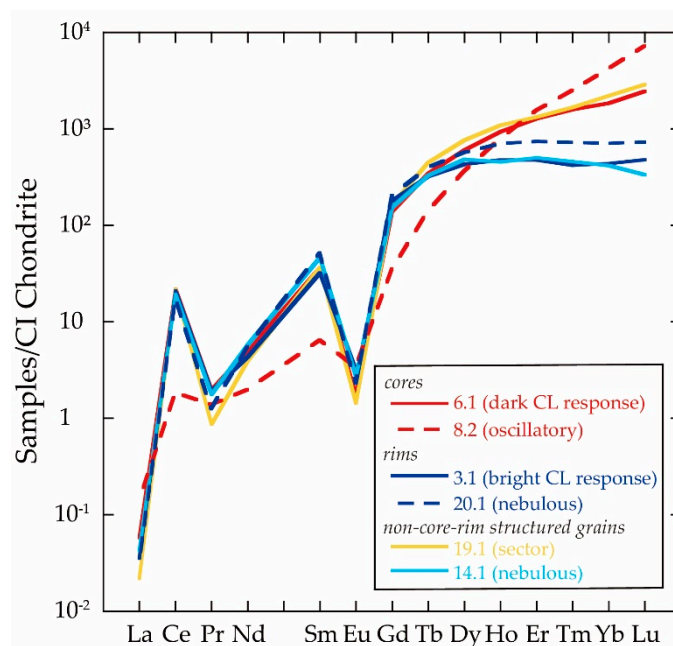
Figure 5. Typical REE abundance patterns normalized by C1-chondrite values [47] of YH05021606A zircons.

3.4. Oxygen Isotope Ratio in Zircon

Oxygen isotope ratios ($\delta^{18}O$) in the YH05021606A zircons were obtained from the same locations as for the U–Pb and REE analyses after re-polishing, and the oxygen isotope data of 53 spots on 45 zircon grains are shown in Table S1, which shows the whole $\delta^{18}O$ data range from 4.97‰ to 6.04‰. $\delta^{18}O$ obtained from the core and rim range from 4.97‰ to 5.91‰ and 4.99‰ to 6.04‰, respectively. $\delta^{18}O$ of the individual grains with no apparent core-rim structure ranges from 5.04‰ to 5.96‰. $\delta^{18}O$ in the zircon exhibits no difference among the various textures in the CL images considering the uncertainties (Table S1).
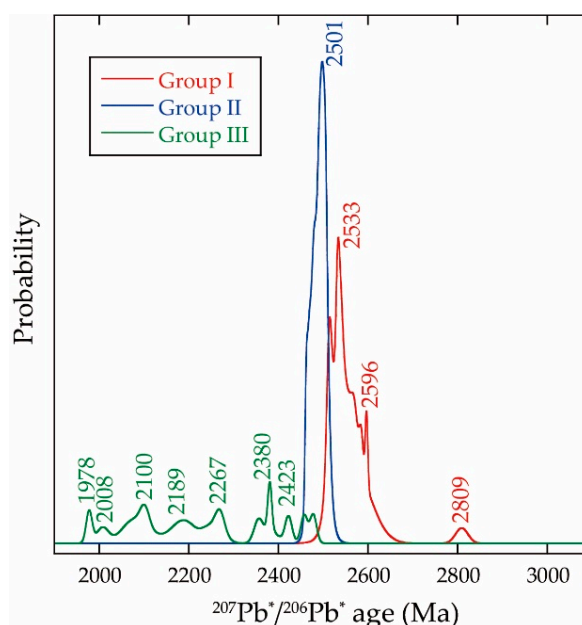
4. Discussion

4.1. Zircon Classification Based on CL Observation and Age Distribution

Based on CL observations, the analytical domains in the zircon grains of the YH05021606A sample can be divided into the following two groups as the first step. The first group, which can be found in the core, is characterized by broad zoning with a dark CL response, oscillatory zoning, or sector zoning. The oscillatory and sector zoning infers igneous origin [45], which indicates that the protolith contained igneous inheritance. The second group, which can be found in the rim, is characterized by broad zoning with a bright CL response or nebulous to fir-tree structures. The nebulous to fir-tree structure is commonly observed in zircons collected from granulite facies rocks [45,48], and the rims were crystallized during the regional high-temperature metamorphism.

As shown in Figures 4 and 6, the U–Pb data of the first group are scattered from 2809 Ma to 1978 Ma and have the largest age peak at 2533 Ma, whereas those of the second group show an age peak at 2501 Ma with younger age components (2355 Ma, 2237 Ma, 2199 Ma, 2175 Ma, 2102 Ma, and 2008 Ma; Table S1). The metamorphic overgrowth or recrystallized age of 2501 Ma is consistent with the previously reported timing of the UHT metamorphism [9–14]. Assuming that the age of 2501 Ma obtained from the second group is the timing of the regional metamorphism, the first group should be older than 2501 Ma; however, as shown in Table S1, it contains younger components (2478 Ma, 2457 Ma, 2423 Ma, 2382 Ma, 2381 Ma, 2270 Ma, 2263 Ma, 2145 Ma, 2099 Ma, 2084 Ma, 2061 Ma, and 1978 Ma). Therefore, the first group components younger than 2501 Ma and the second group

components younger than 2450 Ma, which is the lower limit of the age peak at 2501 Ma, should be grouped together as a younger age group.

Figure 6. Probability density diagram of ^{207}Pb*/^{206}Pb* age of each group.

Based on the above discussion, the analytical domains in cores, rims, and non-core-rim structured grains can be classified into the following three groups (Table 1). Group I consists of domains with an oscillatory, sector, or dark CL broad zoning older than 2501 Ma. Group II consists of domains with a nebulous to fir-tree structure or bright CL broad zoning around 2501 Ma. Group III consists of domains with an oscillatory, sector, or dark CL broad zoning younger than 2501 Ma and domains with a nebulous to fir-tree structure or bright CL broad zoning younger 2450 Ma.

Table 1. Classification of the analytical domains in the YH05021606A zircons.

| Classification	CL Image	U–Pb Age
Group I	oscillatory-zoning, sector-zoning, and dark CL broad zoning	older than 2501 Ma
Group II	nebulous to fir-tree zoning and bright CL broad zoning	around 2501 Ma
Group III *	oscillatory-zoning, sector-zoning, and dark CL broad zoning or nebulous to fir-tree zoning and bright CL broad zoning	younger than 2501 Ma or younger than 2450 Ma

* The domains of Group III satisfy both conditions.

### 4.2. Timing of the UHT Metamorphism

The U–Pb data of the YH05021606A zircons collected from Fyfe Hills of the Napier Complex reveal a consistent age distribution with those reported in [9]; however, many age peaks older than 2600 Ma were absent in the present study. Conversely, we report several age peaks younger than 2400 Ma, which were not detected in the previous study. This difference is probably due to the selection of target zircons because more transparent zircons were selected for investigating the chemical properties of UHT zircon in the present study.

As shown in Figure 6, the U–Pb data of ca. 2501 Ma for Group II is consistent with the previously reported timing of the UHT metamorphism [9–14]. The C1-chondrite-normalized REE patterns obtained from Group II are characterized by a weak fractionation between MREE and HREE, namely lower HREE/MREE (Figures 7 and 8). The REE patterns with flat MREE–HREE are found in the

zircon that grows or is modified in equilibrium with garnets [13,15–17]. The quartzo-feldspathic gneiss (YH05021606A) contains porphyroblastic garnet (Figure 2), and the REE patterns of Group II reflect the zircon overgrowth or recrystallization under high temperature and in equilibrium with garnet. Therefore, the quartzo-feldspathic gneiss experienced high-temperature metamorphism at ca. 2501 Ma. The Th/U ratios of Group II are scattered from 0.07 to 1.65 (Table S1) and consistent with those of the components of the 2518 Ma peak in [9]. Previous works suggest that domains with Th/U ratios lower than 0.1 can be interpreted as forming during high-grade metamorphism because, under these conditions, non-essential structural constituent cations are purged from the recrystallized structure [49], and Th is consumed by crystallization of Th-rich minerals such as monazite [50–52]. A previous study [9] reported that other Fyfe Hills samples contain monazite as an accessory mineral, whereas the quartzo-feldspathic gneiss (YH05021606A) does not contain monazite. The moderate Th/U ratios of Group II are derived from the lack of crystallization of monazite.
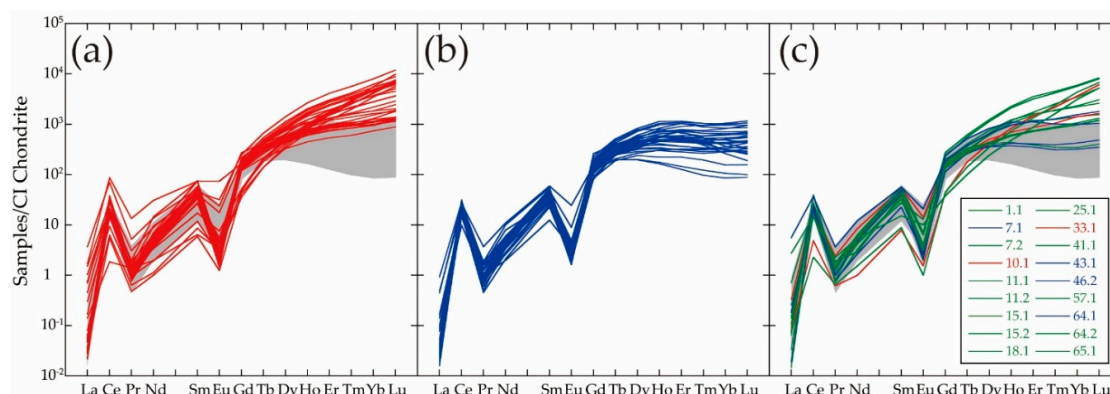
Figure 7. C1-chondrite-normalized REE abundance patterns of (**a**) Group I, (**b**) Group II, and (**c**) Group III.
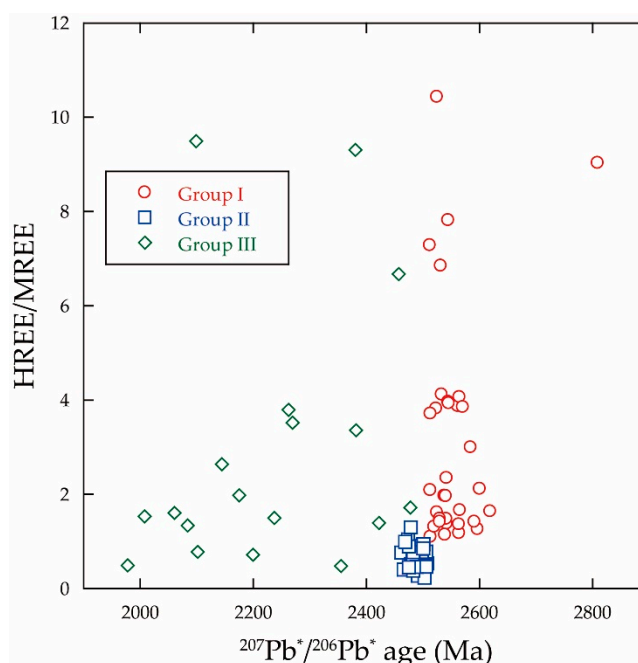
Figure 8. ^{207}Pb*/^{206}Pb* age vs. heavy REE (HREE)/middle REE (MREE) ratio. HREE: Tm + Yb + Lu; MREE: Gd + Tb + Dy.

The youngest age peak obtained from Group I is ca. 2533 Ma (Figure 6). The grains with oscillatory- or sector-zoned structures (Figure 3a,d,e) are the main constituent of the youngest age peak, which indicates that the protolith contained 2533 Ma igneous detritus [45]. The 2533 Ma igneous detritus

is a new component of the Neoarchean magmatic protolith in the Napier Complex. The Th/U ratios of Group I (0.03–1.74) are similar to those of Group II. As shown in Figure 7a, the C1-chondrite-normalized REE patterns of the domains of Group I are multifarious and reflect the chemical composition of their origin. The HREE/MREE ratios of the domains of Group I (32–1505) are notably higher than those of Group II (Figure 8), which suggests that the REE patterns are useful for identifying high-grade metamorphic zircons. Therefore, the UHT metamorphism in Fyfe Hills occurred after 2533 Ma, which is the latest igneous component in the YH05021606A sample, and the metamorphic overgrowth or recrystallization of zircon occurred at 2501 Ma under high temperature conditions.

4.3. Interpretation of Post Metamorphic Ages

The U–Pb data of Group III are scattered from 2478 Ma to 1978 Ma (Figure 6). The geological event(s) after the UHT metamorphism was not reported by previous field-based studies, but similar ages have occasionally been reported for the Napier Complex [53–57]. An age of ca. 2380 Ma was reported based upon Sm–Nd systematics at Mt. Riiser-Larsen area [55]. U–Pb chemical age using an electron microprobe of ca. 2200 Ma obtained for beryllium syn-metamorphic pegmatites at Khmara Bay area reflects post-emplacement deformation and metamorphism [53]. Alteration selvedge adjacent to early Palaeozoic pegmatite in Tonagh Island contains ca. 1930–1800 Ma zircon grains [56]. [56] pointed out that zircon isotopic systematics might be easily disturbed, resulting in radiogenic Pb loss with complete or significant isotopic resetting via local fluid infiltration or pervasive deformation. Several chemical Th–U–total Pb isochron (CHIME) ages from monazite and xenotime in the Napier Complex provide independent confirmation of an isotopic disturbance after the UHT metamorphism [53,54]. A previous study [9] also reported ages of 2280 Ma, 2198 Ma, and 1824 Ma in the felsic orthogneiss collected from Fyfe Hills and suggested that the younger age distribution represents a disturbance of the U–Pb system in zircon grains by local fluid infiltration or local deformation event(s).

The C1-chondrite-normalized REE patterns of Group III are shown in Figure 7c. The ages of spots 10.1 and 33.1 are 2478 ± 7 Ma and 2457 ± 7 Ma (Table S1), respectively, which are consistent with the age of Group II, whereas the REE patterns of spots 10.1 and 33.1 (Figure 7c) are similar to those of Group I. The CL image and REE pattern indicate that spots 10.1 and 33.1 are the domains of Group I (Table S1); therefore, both spots should be omitted from the age estimation of the local metamorphism. The REE patterns of spots 7.1, 43.1, 46.2, and 64.1 are similar to those of Group II (Figure 7c), and their HREE/MREE ratios (0.48, 0.72, 0.78, and 1.53, respectively; Table S2) are consistent with those of Group II. The CL image and REE pattern suggest the similarity of spots 7.1, 43.1, 46.2, and 64.1 with Group II (Tables S1 and S2). In addition, the core (spot 10.1: 2478 ± 7 Ma) of grain no. YH1606A-10 is younger than the rim (spot 10.2: 2502 ± 7 Ma) (Figure 3b), which indicates radiogenic Pb loss from the core. Therefore, the younger age distribution results in a disturbance of the U–Pb system in the domains of Group I and II.

4.4. Oxygen Isotope in High-Grade Metamorphic Zircons

The zircon oxygen isotope record in the inherited cores is generally preserved despite other minerals that have been disturbed by high-grade metamorphism because of the slower diffusion rate [18,58]. $\delta^{18}O$ in the overgrowth and recrystallization domains results from oxygen isotope exchange with the host rock during sub-solidus processes. Conversely, some previous studies reported the possibility of oxygen isotope exchange between the core and rim during high temperature (e.g., [59]).

Judging from U–Pb ages and REE compositions, the YH05021606A zircons have multiple origins, predicting varied $\delta^{18}O$. However, the oxygen isotope analyses yielded relatively homogeneous $\delta^{18}O$ among the three groups (Figure 9). The average $\delta^{18}O$ of Group I, II, and III is 5.53 ± 0.11‰, 5.51 ± 0.14‰, and 5.53 ± 0.23‰, respectively, which is consistent with that of zircon in equilibrium with the mantle materials (5.3 ± 0.3‰: [18]). It is uncommon that multiple components in the protolith have similar $\delta^{18}O$. In addition, $\delta^{18}O$ of the rim is equal to that of the core because $\delta^{18}O$ of the rim results from oxygen isotope exchange with the host rock. A previous study reported that zircon oxygen isotope composition

was re-equilibrated with metamorphic fluids, although the zircon REE composition remained nearly unchanged [60]. $\delta^{18}O$ of the YH05021606A zircons suggests a re-equilibration of oxygen isotopes after metamorphism at ca. 2501 Ma. The YH05021606A sample does not include hydrous minerals and, as such, provides a valuable opportunity to investigate oxygen diffusion in zircon under dry conditions. Further studies are necessary to interpret oxygen diffusion under different H_2O activities.
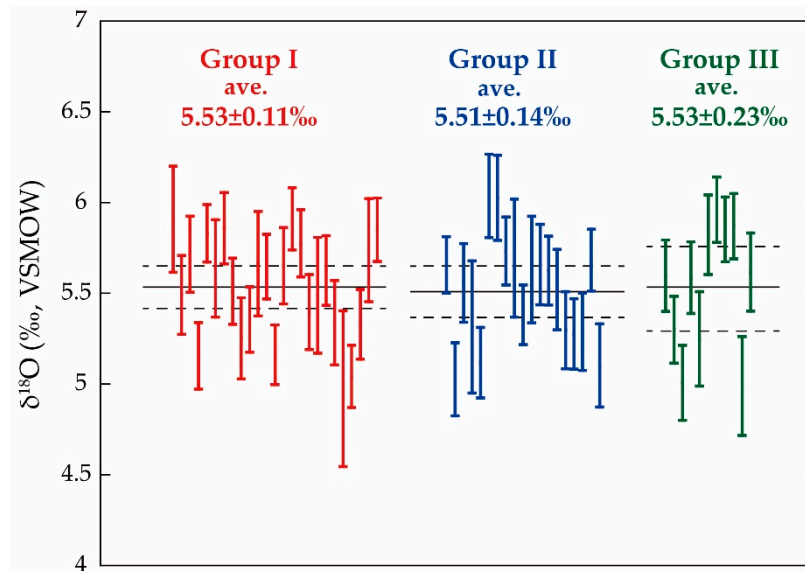
Figure 9. $\delta^{18}O_{VSMOW}$ of YH05021606A zircons. The classification corresponds to the classification in Table 1. Error bars indicate 95% confidence. Black lines indicate the averages, and black dotted lines indicate the 95% confidence error ranges of the data of each classification.

5. Conclusions

U–Pb dating, REE abundance measurement, and oxygen isotope analysis were performed on zircon grains in garnet-bearing quartzo-feldspathic gneiss (YH05021606A) from Fyfe Hills in the Napier Complex, and the following conclusions can be made.

(i)　Combining CL observation and dating allows us to classify analytical domains into three groups.

(ii)　Group I comprises inheritance older than 2501 Ma.

(iii)　Group II comprises metamorphic overgrowth and recrystallization at 2501 Ma.

(iv)　Group III is caused by the disturbance of the U–Pb system in Group I and II.

(v)　The UHT metamorphism in Fyfe Hills occurred after 2533 Ma, which is the newfound igneous components, and the metamorphic overgrowth or recrystallization of zircon occurred at 2501 Ma under high temperature conditions.

(vi)　REE abundance is a useful indicator of metamorphic zircon in garnet-bearing gneiss, whereas the Th/U ratio is not always useful.

(vii)　Oxygen isotope composition in zircon re-equilibrated after metamorphism under dry UHT conditions.

Conflicts of Interest: The authors declare no conflict of interest.

References

1. Kelsey, D.E.; Hand, M. On ultrahigh temperature crustal metamorphism: Phase equilibria, trace element thermometry, bulk composition, heat sources, timescales and tectonic settings. *Geosci. Front.* **2015**, *6*, 311–356.

2. Dallwitz, W.B. Co-existing sapphirine and quartz in granulite from Enderby Land, Antarctica. *Nature* **1968**, *219*, 476–477.

3. Harley, S.L. A matter of time: The importance of the duration of UHT metamorphism. *J. Mineral. Petrol. Sci.* **2016**, *111*, 50–72.

4. Harley, S.L.; Kinny, P.D.; Snape, I.; Black, L.P. Zircon chemistry and the definition of events in Archaean granulite terrains. In Proceedings of the Fourth International Archaean Symposium, Perth, Australia, 24–28 September 2001.

5. Crowe, W.; Osanai, Y.; Toyoshima, T.; Owada, M.; Tsunogae, T.; Hokada, T. SHRIMP geochronology of a mylonite zone on Tonagh Island: Characterisation of the last high-grade tectonothermal event in the Napier Complex, East Antarctica. *Polar Geosci.* **2002**, *15*, 17–36.

6. Kelly, N.M.; Harley, S.L. An integrated microtextural and chemical approach to zircon geochronology: Refining the Archaean history of the Napier Complex, east Antarctica. *Contrib. Mineral. Petrol.* **2005**, *149*, 57–84.

7. Clark, C.; Taylor, R.J.; Kylander-Clark, A.R.; Hacker, B.R. Prolonged (>100 Ma) ultrahigh temperature metamorphism in the Napier Complex, East Antarctica: A petrochronological investigation of Earth's hottest crust. *J. Metamorph. Geol.* **2018**, *36*, 1117–1139.

8. Król, P.; Kusiak, M.A.; Dunkley, D.J.; Wilde, S.A.; Yi, K.; Lee, S.; Kocjan, I. Diversity of Archean crust in the eastern Tula Mountains, Napier Complex, East Antarctica. *Gondwana Res.* **2020**, *82*, 151–170.

9. Horie, K.; Hokada, T.; Hiroi, Y.; Motoyoshi, Y.; Shiraishi, K. Contrasting Archaean crustal records in western part of the Napier Complex, East Antarctica: New constraints from SHRIMP geochronology. *Gondwana Res.* **2012**, *21*, 829–837.

10. Grew, E.S. Boron and beryllium minerals in granulite-facies pegmatites and implications of beryllium pegmatites for the origin and evolution of the Archean Napier Complex of East Antarctica. *Mem. Natl. Inst. Polar Res. Spec. Issue* **1998**, *53*, 74–92.

11. Carson, C.J.; Ague, J.J.; Coath, C.D. U–Pb geochronology from Tonagh Island, East Antarctica: Implications for the timing of ultra-high temperature metamorphism of the Napier Complex. *Precambrian Res.* **2002**, *116*, 237–263.

12. Hokada, T.; Misawa, K.; Shiraishi, K.; Suzuki, S. Mid to late Archaean (3.3–2.5 Ga) tonalitic crustal formation and high-grade metamorphism at Mt. Riiser-Larsen, Napier Complex, East Antarctica. *Precambrian Res.* **2003**, *127*, 215–228. [CrossRef]

13. Hokada, T.; Harley, S.L. Zircon growth in UHT leucosome: Constraints from zircon-garnet rare earth elements (REE) relations in Napier Complex, East Antarctica. *J. Mineral. Petrol. Sci.* **2004**, *99*, 180–190. [CrossRef]

14. Suzuki, S.; Arima, M.; Williams, I.S.; Shiraishi, K.; Kagami, H. Thermal history of UHT metamorphism in the Napier Complex, East Antarctica: Insights from zircon, monazite, and garnet ages. *J. Geol.* **2006**, *114*, 65–84. [CrossRef]

15. Rubatto, D. Zircon trace element geochemistry: Partitioning with garnet and the link between U-Pb ages and metamorphism. *Chem. Geol.* **2002**, *184*, 123–138. [CrossRef]

16. Fornelli, A.; Langone, A.; Micheletti, F.; Pascazio, A.; Piccarreta, G. The role of trace element partitioning between garnet, zircon and orthopyroxene on the interpretation of zircon U–Pb ages: An example from high-grade basement in Calabria (Southern Italy). *Int. J. Earth Sci.* **2014**, *103*, 487–507. [CrossRef]

17. Fornelli, A.; Langone, A.; Micheletti, F.; Piccarreta, G. REE partition among zircon, orthopyroxene, amphibole and garnet in a high-grade metabasic system. *Geol. Mag.* **2018**, *155*, 1705–1726. [CrossRef]

18. Valley, J.W. Oxygen isotopes in zircon. *Rev. Mineral. Geochem.* **2003**, *53*, 343–385.
19. Trail, D.; Tailby, N.; Wang, Y.; Mark Harrison, T.; Boehnke, P. Aluminum in zircon as evidence for peraluminous and metaluminous melts from the H adean to present. *Geochem. Geophys. Geosystems* **2017**, *18*, 1580–1593.
20. Takehara, M.; Horie, K.; Hokada, T.; Kiyokawa, S. New insight into disturbance of U–Pb and trace-element systems in hydrothermally altered zircon via SHRIMP analyses of zircon from the Duluth gabbro. *Chem. Geol.* **2018**, *484*, 168–178. [CrossRef]
21. Tang, H.; Trail, D.; Bell, E.A.; Harrison, T.M. Zircon halogen geochemistry: Insights into Hadean-Archean fluids. *Geochem. Perspect. Lett.* **2019**, *9*, 49–53. [CrossRef]
22. Harley, S.L.; Motoyoshi, Y. Al zoning in orthopyroxene in a sapphirine quartzite: Evidence for >1120 °C UHT metamorphism in the Napier Complex, Antarctica, and implications for the entropy of sapphirine. *Contrib. Mineral. Petrol.* **2000**, *138*, 293–307. [CrossRef]
23. Hokada, T. Feldspar thermometry in ultrahigh-temperature metamorphic rocks: Evidence of crustal metamorphism attaining ~ 1100 C in the Archean Napier Complex, East Antarctica. *Am. Mineral.* **2001**, *86*, 932–938. [CrossRef]
24. Ishizuka, H.; Suzuki, S.; Nakamura, A. Peak temperatures of ultra-high temperature metamorphism of the Napier Complex, Enderby Land, East Antarctica, as deduced from porphyroclastic pyroxenes of meta-ultramafic rocks. *Polar Geosci.* **2002**, *15*, 1–16.
25. Williams, I.S.; Compston, W.; Black, L.P.; Ireland, T.R.; Foster, J.J. Unsupported radiogenic Pb in zircon: A cause of anomalously high Pb-Pb, U-Pb and Th-Pb ages. *Contrib. Mineral. Petrol.* **1984**, *88*, 322–327. [CrossRef]
26. Black, L.P.; Williams, I.S.; Compston, W. Four zircon ages from one rock: The history of a 3930 Ma-old granulite from Mount Sones, Enderby Land, Antarctica. *Contrib. Mineral. Petrol.* **1986**, *94*, 427–437. [CrossRef]
27. Harley, S.L.; Black, L.P. A revised Archaean chronology for the Napier Complex, Enderby Land, from SHRIMP ion-microprobe studies. *Antarct. Sci.* **1997**, *9*, 74–91. [CrossRef]
28. Kusiak, M.A.; Whitehouse, M.J.; Wilde, S.A.; Dunkley, D.J.; Menneken, M.; Nemchin, A.A.; Clark, C. Changes in zircon chemistry during Archean UHT metamorphism in the Napier Complex, Antarctica. *Am. J. Sci.* **2013**, *313*, 933–967. [CrossRef]
29. Kusiak, M.A.; Whitehouse, M.J.; Wilde, S.A.; Nemchin, A.A.; Clark, C. Mobilization of radiogenic Pb in zircon revealed by ion imaging: Implications for early Earth geochronology. *Geology* **2013**, *41*, 291–294. [CrossRef]
30. Takehara, M.; Horie, K.; Hokada, T.; Kiyokawa, S. Data on recovery rates and external morphologies of zircon grains from mechanical and electrical pulverization of rock samples. *Data Brief* **2018**, *19*, 1537–1544. [CrossRef]
31. Black, L.P.; Kamo, S.L.; Allen, C.M.; Davis, D.W.; Aleinikoff, J.N.; Valley, J.W.; Mundil, R.; Campbell, I.H.; Korsch, R.J.; Williams, I.S.; et al. Improved ^{206}Pb/^{238}U microprobe geochronology by the monitoring of a trace-element-related matrix effect; SHRIMP, ID–TIMS, ELA–ICP–MS and oxygen isotope documentation for a series of zircon standards. *Chem. Geol.* **2004**, *205*, 115–140. [CrossRef]
32. Paces, J.B.; Miller, J.D. Precise U–Pb ages of Duluth complex and related mafic intrusions, northeastern Minnesota: Geochronological insights to physical, petrogenetic, paleomagnetic, and tectonomagmatic processes associated with the 1.1 Ga midcontinent rift system. *J. Geophys. Res. Solid Earth* **1993**, *98*, 13997–14013. [CrossRef]
33. Wiedenbeck, M.; Alle, P.; Corfu, F.; Griffin, W.L.; Meier, M.; Oberli, F.; Vonquadt, A.; Roddick, J.C.; Spiegel, W. Three natural zircon standards for U-Th-Pb, Lu-Hf, trace element and REE analyses. *Geostand. Newsl.* **1995**, *19*, 1–23. [CrossRef]
34. Williams, I.S. U–Th–Pb Geochronology by Ion Microprobe. In *Applications of Microanalytical Techniques to Understanding Mineralizing Processes: Reviews in Economic Geology*; McKibben, M.A., Shanks, W.C., III, Ridley, W.I., Eds.; Society of Economic Geologists: Lyttelton, CO, USA, 1997; Volume 7, pp. 1–35.
35. Ludwig, K.R. *SQUID 2: A User's Manual*; Berkeley Geochronology Center Special Publication: Berkeley, CA, USA, 2009; Volume 2, p. 104.
36. Stacey, J.S.; Kramers, J.D. Approximation of terrestrial lead isotope evolution by a two-stage model. *Earth Planet. Sci. Lett.* **1975**, *26*, 207–221. [CrossRef]
37. Ludwig, K.R. *Isoplot 3.75-4.15: A Geochronological Toolkit for Microsoft Excel*; Berkeley Geochronology Center Special Publication: Berkeley, CA, USA, 2012.

38. Williams, I.S.; Hergt, J.M. U–Pb Dating of Tasmanian Dolerites: A Cautionary Tale of SHRIMP Analysis of High-U Zircon. In *Beyond 2000: New Frontiers in Isotope Geoscience*; Woodhead, J.D., Hergt, J.M., Nobel, W.P., Eds.; University of Melbourne: Melbourne, Australia, 2000; pp. 185–188.

39. Butera, K.M.; Williams, I.S.; Blevin, P.L.; Simpson, C.J. Zircon U–Pb dating of early Palaeozoic monzonitic intrusives from the Goonumbla area, New South Wales. *Aust. J. Earth Sci.* **2001**, *48*, 457–464. [CrossRef]

40. Maas, R.; Kinny, P.D.; Williams, I.S.; Froude, D.O.; Compston, W. The Earth's oldest known crust: A geochronological and geochemical study of 3900–4200 Ma old detrital zircons from Mt. Narryer and Jack Hills, Western Australia. *Geochim. Cosmochim. Acta* **1992**, *56*, 1281–1300. [CrossRef]

41. Horie, K.; Hidaka, H.; Gauthier-Lafaye, F. Elemental distribution in zircon: Alteration and radiation-damage effects. *Phys. Chem. EarthParts A/B/C* **2006**, *31*, 587–592. [CrossRef]

42. Horie, K.; Takehara, M.; Suda, Y.; Hidaka, H. Potential Mesozoic reference zircon from the Unazuki plutonic complex: Geochronological and geochemical characterization. *Isl. Arc* **2013**, *22*, 292–305. [CrossRef]

43. Wiedenbeck, M.; Hanchar, J.M.; Peck, W.H.; Sylvester, P.; Valley, J.; Whitehouse, M.; Kronz, A.; Morishita, Y.; Nasdala, L.; Franchi, I.; et al. Further characterisation of the 91500 zircon crystal. *Geostand. Geoanalytical Res.* **2004**, *28*, 9–39. [CrossRef]

44. Ickert, R.B.; Hiess, J.; Williams, I.S.; Holden, P.; Ireland, T.R.; Lanc, P.; Schram, H.; Foster, J.J.; Clement, S.W. Determining high precision, in situ, oxygen isotope ratios with a SHRIMP II: Analyses of MPI-DING silicate-glass reference materials and zircon from contrasting granites. *Chem. Geol.* **2008**, *257*, 114–128. [CrossRef]

45. Corfu, F.; Hanchar, J.M.; Hoskin, P.W.; Kinny, P. Atlas of zircon textures. *Rev. Mineral. Geochem.* **2003**, *53*, 469–500. [CrossRef]

46. Song, B.; Nutman, A.P.; Liu, D.; Wu, J. 3800 to 2500 Ma crustal evolution in the Anshan area of Liaoning Province, northeastern China. *Precambrian Res.* **1996**, *78*, 79–94. [CrossRef]

47. McDonough, W.F.; Sun, S.S. The composition of the Earth. *Chem. Geol.* **1995**, *120*, 223–253. [CrossRef]

48. Pidgeon, R.T.; Nemchin, A.A.; Kinny, P.D. Fir-tree and nebulously zoned zircons from granulite facies rocks: Evidence for zircon growth and interaction with metamorphic fluids. Goldschmidt 2000. *Conf. Abstr.* **2000**, *5*, 798.

49. Hoskin, P.W.O.; Black, L.P. Metamorphic zircon formation by solid-state recrystallization of protolith igneous zircon. *J. Metamorph. Geol.* **2000**, *18*, 423–439. [CrossRef]

50. Williams, I.S.; Claesson, S. Isotopic evidence for the Precambrian provenance and Caledonian metamorphism of high grade paragneisses from the Seve Nappes, Scandinavian Caledonides. *Contrib. Mineral. Petrol.* **1987**, *97*, 205–217. [CrossRef]

51. Schiøtte, L.; Compston, W.; Bridgwater, D. U–Th–Pb ages of single zircons in Archaean supracrustals from Nain Province, Labrador, Canada. *Can. J. Earth Sci.* **1989**, *26*, 2636–2644. [CrossRef]

52. Kinny, P.D.; Wijbrans, J.R.; Froude, D.O.; Williams, I.S.; Compston, W. Age constraints on the geological evolution of the Narryer Gneiss Complex, Western Australia. *Aust. J. Earth Sci.* **1990**, *37*, 51–69. [CrossRef]

53. Grew, E.S.; Suzuki, K.; Asami, M. CHIME ages of xenotime, monazite and zircon from beryllium pegmatites in the Napier Complex, Khmara Bay, Enderby Land, East Antarctica. *Polar Geosci.* **2001**, *14*, 99–118.

54. Owada, M.; Osanai, Y.; Tsunogae, T.; Hamamoto, T.; Kagami, H.; Toyoshima, T.; Hokada, T. Sm-Nd garnet ages of retrograde garnet bearing granulites from Tonagh Island in the Napier Complex, East Antarctica: A preliminary study. *Polar Geosci.* **2001**, *14*, 75–87.

55. Suzuki, S.; Kagami, H.; Ishizuka, H.; Hokada, T. Sm-Nd mineral isochron age of sapphirine-quartz gneiss from the Mt. Riiser-Larsen area in the Napier Complex, East Antarctica. *Polar Geosci.* **2001**, *14*, 88–98.

56. Carson, C.J.; Ague, J.J.; Grove, M.; Coath, C.D.; Harrison, T.M. U–Pb isotopic behaviour of zircon during upper-amphibolite facies fluid infiltration in the Napier Complex, east Antarctica. *Earth Planet. Sci. Lett.* **2002**, *199*, 287–310. [CrossRef]

57. Hokada, T.; Motoyoshi, Y. Electron Microprobe Technique for U-Th-Pb and REE Chemistry of Monazite, and its Implications for pre-, Peak-and Post-Metamorphic Events of the Lutzow-Holm Complex and the Napier Complex, East Antarctica. *Polar Geosci.* **2006**, *19*, 118–151.

58. Peck, W.H.; Valley, J.W.; Graham, C.M. Slow oxygen diffusion rates in igneous zircons from metamorphic rocks. *Am. Mineral.* **2003**, *88*, 1003–1014. [CrossRef]

59. Claesson, S.; Bibikova, E.V.; Shumlyanskyy, L.; Whitehouse, M.J.; Billström, K. Can oxygen isotopes in magmatic zircon be modified by metamorphism? A case study from the Eoarchean Dniester-Bug Series, Ukrainian Shield. *Precambrian Res.* **2016**, *273*, 1–11. [CrossRef]

60. Roberts, N.M.; Yang, Q.Y.; Santosh, M. Rapid oxygen diffusion during high temperature alteration of zircon. *Sci. Rep.* **2018**, *8*, 1–10. [CrossRef]

Publisher's Note: MDPI stays neutral with regard to jurisdictional claims in published maps and institutional affiliations.